DRAFT VERSION FEBRUARY 12, 2022
Preprint typeset using LaTeX style emulateapj v. 5/2/11

arXiv:1512.03453v1 [astro-ph.SR] 10 Dec 2015

THE INTERPLAY BETWEEN CHEMISTRY AND NUCLEATION IN THE FORMATION OF CARBONACEOUS DUST IN SUPERNOVA EJECTA

DAVIDE LAZZATI[1], ALEXANDER HEGER[2,3,4,5]

Draft version February 12, 2022

ABSTRACT

Core-collapse supernovae are considered to be important contributors to the primitive dust enrichment of the interstellar medium in the high-redshift universe. Theoretical models of dust formation in stellar explosions have so far provided controversial results and a generally poor fit to the observations of dust formation in local supernovae. We present a new methodology for the calculation of carbonaceous dust formation in young supernova remnants. Our new technique uses both the nucleation theory and a chemical reaction network to allow us to compute the dust growth beyond the molecular level as well as to consider chemical erosion of the forming grains. We find that carbonaceous dust forms efficiently in the core of the ejecta, but takes several years to condensate, longer than previously estimated. It forms unevenly and remains concentrated in the inner part of the remnant. These results support the role of core-collapse supernovae as dust factories and provide new insight on the observations of SN 1987A, in which large amounts of dust have been detected to form on a timescale of years after core collapse.

Subject headings: galaxies: ISM: dust — ISM: supernova remnants — ISM: molecules — supernovae: general

1. INTRODUCTION

The observations of significant amounts of dust in high redshift quasars (Bertoldi et al. 2003; Priddey et al. 2003; Robson et al. 2004; Beelen et al. 2006; Wang et al. 2008) have highlighted the requirement for an alternative to asymptotic giant branch (AGB) stars as the dominant dust factories in the early Universe (e.g., Maiolino et al. 2004, Valiante et al. 2009, 2011). An ideal alternative are core-collapse supernovae (CCSNe), since the short main sequence time of their progenitor stars allows them to enrich the interstellar medium with the first solids with no noticeable delay on cosmological timescales.

Theoretical calculations of the dust yields of CCSNe, however, have produced controversial results. Calculations based on the classical nucleation theory (e.g., Feder et al. 1966) typically predict the prompt formation of fairly large amounts of dust, of the order of one solar mass or more, within one year from the explosion (Kozasa et al. 1989, 1991; Clayton et al. 2001; Todini & Ferrara 2001; Nozawa et al. 2003, 2010). The result is robust to the unknown parameters of the theory, such as the shape and sticking coefficients of the grains, at least to first order (Fallest et al. 2013). On the other hand, calculations that model the formation of solid grains with a chemical network with well-defined reaction rates resulted in the prediction of only modest amount of dust, its condensation starting only years after the supernova explosion (Cherchneff & Dwek 2009, 2010; Sarangi & Cherchneff 2013; Biscaro & Cherchneff 2014). Such calculations, however, cannot follow the grain formation up to large molecular clusters and/or micron-sized crystals. Most current results only predict the formation of molecular precursors, such as C_{12}. A recent paper (Sarangi et al. 2015) follows carbon cluster formation up to C_{28}, assuming that coalescence is responsible for the growth of astrophysical grains from the clusters.

The discrepancy between the two theoretical predictions seems to be brought about by the approximations and intrinsic limitations of the two theories. Calculations based on the nucleation theory assume that the grain formation happens in virtual isolation, ignoring the fact that the growing proto-grains are exposed to the rich field of damaging radiation of a young supernova remnant (SNR). They also assume that even the smallest molecular clusters are continuum entities, ignoring their atomic structure and quantum behaviour. On the other hand, chemical network calculations provide a deterministic growth of grains and therefore ignore the fact that, as grains grow beyond the molecular cluster phase, self shielding allow the few grains that grew by statistical fluctuations to become more and more resilient and grow even further. Chemical calculations, as such, ignore the fact that grain growth becomes a runaway process, the few grains able to make it beyond a few hundred monomers allowed to grow and become stable.

Not surprisingly, observations of nearby core-collapse supernovae (SN1987A and, only recently, SN2010jl) are in disagreement with both results. They show dust formation beginning as early as half a year after the explosion (Gall et al. 2014; earlier dust formation being possible but hidden under the more abundant curcumstellar dust component), in disagreement with chemical network results. The early dust formation, however, is modest, at most a fraction of a per cent of a solar mass being condensed (in disagreement with the classical nucleation results). To add confusion to the picture, recent Herschel (Matsuura et al. 2013) and ALMA (Indebetouw et al. 2014) observations of SN1987A show the presence of large amounts of dust in emission in the center of the remnant. Taken at face value, the collective data from all nearby core-collapse supernovae suggests a scenario in which dust formation is a slow and continuous process that starts at most

[1] Department of Physics, Oregon State University, 301 Weniger Hall, Corvallis, OR 97331, U.S.A.
[2] Monash Center for Astrophysics, School of Physics and Astronomy, Monash University, Vic 3800, Australia
[3] School of Physics & Astronomy, University of Minnesota, Minneapolis, MN 55455, U.S.A.
[4] Joint Institute for Nuclear Astrophysics, 225 Nieuwland Science Hall Department of Physics, University of Notre Dame, Notre Dame, IN 46556, U.S.A.
[5] Center for Nuclear Astrophysics, Department of Physics and Astronomy, Shanghai Jiao-Tong University, Shanghai 200240, P. R. China.

a few months after core collapse and continues for at least several years, eventually yielding amounts of solid particles totalling approximately one solar mass. Not all core-collapse supernovae may be dust producers, however. In a recent study, Szalai & Vinkó (2013) find that only two out of twelve type II-P SNe show signs of newly sinthsized dust in emission.

Connecting the chemistry of the molecular precursor with a formalism for dust growth is necessary to properly describe the formation and growth of grains into stable microscopic solids (Sarangi & Cherchneff 2015). In this paper we present a new framework for the calculation of dust formation in supernova explosions based on the kinetic nucleation theory (e.g., Kashchiev 2000). Whereas the kinetic nucleation theory is equivalent to the standard thermodynamic theory for homologous nucleation in isolation, it allows to introduce deviations from the capillary approximation for very small clusters and chemical weathering of the forming grains in the harsh supernova environment. The theory is presented, and applied as a proof of concept, to the formation of carbonaceous grains, but can be readily extended to the formation of any grain species, provided that its susceptibility to weathering in the remnant environment is known.

This paper is organized as follows: in Section 2 we present the chemical network and the nucleation theory that we adopt. In Section 3 we describe the stellar explosions model adopted and in Section 4 we present out results. A summary and discussion are in Section 5.

2. CHEMISTRY AND DUST FORMATION PHYSICS

This work is based on a small chemical and dust nucleation network aimed at keeping track of the concentrations of CO molecules, free oxygen and carbon atoms, hydrogen and helium cations, thermal and non-thermal free electrons, and carbonaceous grains. In this section we describe the physical processes and the techniques used to compute such concentrations. The reactions considered are:

$$\mathrm{He} + \mathrm{e_C^-} \rightarrow \mathrm{He^+} + \mathrm{e_C^-} + \mathrm{e_T^-} \quad (1)$$
$$\mathrm{He^+} + \mathrm{e_T^-} \rightarrow \mathrm{He} \quad (2)$$
$$\mathrm{H} + \mathrm{e_C^-} \rightarrow \mathrm{H^+} + \mathrm{e_C^-} + \mathrm{e_T^-} \quad (3)$$
$$\mathrm{H^+} + \mathrm{e_T^-} \rightarrow \mathrm{H} \quad (4)$$
$$\mathrm{C} + \mathrm{O} \rightarrow \mathrm{CO} \quad (5)$$
$$\mathrm{CO} \rightarrow \mathrm{C} + \mathrm{O} \quad (6)$$
$$\mathrm{CO} + \mathrm{e_C^-} \rightarrow \mathrm{C} + \mathrm{O} + \mathrm{e_C^-} \quad (7)$$
$$\mathrm{CO} + \mathrm{He^+} \rightarrow \mathrm{O} + \mathrm{He} + \mathrm{C^+} \quad (8)$$
$$\mathrm{C}_n + \mathrm{O} \rightarrow \mathrm{C}_{n-1} + \mathrm{CO} \quad (9)$$
$$\mathrm{C}_n + \mathrm{He^+} \rightarrow \mathrm{C}_{n-1} + \mathrm{He} + \mathrm{C^+} \quad (10)$$
$$\mathrm{C}_n + \mathrm{C} \rightarrow \mathrm{C}_{n+1} \quad (11)$$
$$\mathrm{C}_n \rightarrow \mathrm{C}_{n-1} + \mathrm{C} \quad (12)$$

where $\mathrm{e_C^-}$ is a Compton electron consequence of the energy deposited by the decay of ^{56}Ni into ^{56}Co and eventually ^{56}Fe and $\mathrm{e_T^-}$ is a free electron in thermal equilibrium with the surrounding gas.

Reactions 1 and 2 are the ionization and recombination of He atoms as a consequence of the presence of non-thermal electrons. Reactions 3 and 4 are the ionization and recombination of H atoms as a consequence of the presence of non-thermal electron. Reaction 5 is the formation of carbon monoxide molecules by radiative association, and reactions 6, 7, and 8 are the destruction of the CO molecule due to thermal effects, interaction with non-thermal electrons, and charge-exchange with $\mathrm{He^+}$ cations, respectively. Reactions 9 and 10 are the chemical weathering reactions in which the Carbon clusters or grains lose one carbon atom by reaction with a free oxygen atom (oxidation) or He ion (ion-molecule). Finally, reactions 11 and 12 are the monomer attachment and spontaneous detachment reactions to and from carbon clusters. The network considered here is much smaller than the one used by Cherchneff & Dwek (2009, 2010). In this paper, however, we are focusing on the carbonaceous nucleation only rather than following all possible dust species. In addition, the main goal of this work is to study the interplay between chemistry and nucleation with an hybrid approach that allows us to consider carbon clusters both as molecules, subject to interactions with other species, and as small solids, capable of growing indefinitely.

2.1. *Ionization balance*

To compute the density of free electrons and of the HII and HeII cations, we calculate the balance between the ionization rate due to interaction with Compton electrons and recombination from the bath of thermal electrons. We then use the H and He ionization as a proxy for the ionization of the whole SNR to compute the total density of free electrons.

The ionization rate of the atom or ion X due to collisions with Compton electrons is given by:

$$k_X = L_\gamma / W_X \ , \quad (13)$$

where W_X is the average energy per ionization of the species X (Liu & Victor 1994; Liu & Dalgarno 1995; Cherchneff & Lilly 2008). The luminosity of the ^{56}Ni decay L_γ is given by (e.g., Woosley et al. 1989):

$$L_\gamma = 7.5 \times 10^{-8} \frac{N_{^{56}\mathrm{Ni}}}{N_{\mathrm{tot}}} \langle E_\gamma \rangle f_\gamma(K_{56}) e^{-\frac{t}{\tau_{56}}} \quad \mathrm{MeV\ s^{-1}} \quad (14)$$

where $N_{^{56}\mathrm{Ni}}$ is the total number of ^{56}Ni atoms produced in the SN explosion, N_{tot} is the total number of atoms in the ejecta, $\langle E_\gamma \rangle = 3.57\,\mathrm{MeV}$ is the average energy released in each decay, and $\tau_{56} = 111.26\,\mathrm{d}$ is the e-folding time of ^{56}Co decay. $f_\gamma(K_{56})$, the deposition function, is given by:

$$f_\gamma(K_{56}) = 1 - e^{-K_{56}\phi_0 (t_0/t)^2} \ , \quad (15)$$

where $K_{56} = 0.033$ is the average γ-ray mass absorption coefficient (Woosley et al. 1989), and $\phi_0 = 5 \times 10^4\,\mathrm{g\,cm^{-2}}$ is the mass column density of the ejecta model used in this work at a reference time $t_0 = 10^6\,\mathrm{s}$ (Woosley et al. 1989; Todini & Ferrara 2001). Most of the numerical values used were computed for models of the SN 1987A explosion and may not be strictly appropriate for our computation. Given the overall simplification of the model, however, and especially the assumption of a uniform density of non-thermal electrons throughout the remnant, computing appropriate values for the SN explosion considered here is beyond the scope of the paper. The average energy per ionization of H is (Dalgarno et al. 1999)

$$W_{\mathrm{H}} = 36.1\,\mathrm{eV} \quad (16)$$

and the average energy per ionization of He is

$$W_{\mathrm{He}} = 46.3\,\mathrm{eV} \ . \quad (17)$$

The temperature-dependent recombination rate $\alpha_{\mathrm{r}}(T)$ of free thermal electrons on the hydrogen and helium ions was computed following Verner & Ferland (1996). The recombination

	a (cm^3 s^{-1})	b	T_0	T_1
H	7.982×10^{-11}	0.748	3.148	7.036×10^5
He	9.356×10^{-10}	0.7892	4.266×10^{-2}	4.677×10^6

TABLE 1
PARAMETERS USED IN EQ. 18 TO COMPUTE THE RECOMBINATION RATES OF HYDROGEN AND HELIUM CATIONS.

rate is given (in units of cm^3 s^{-1}) by:

$$\alpha_{\rm r}(T) = a\left[\sqrt{\frac{T}{T_0}}\left(1+\sqrt{\frac{T}{T_0}}\right)^{1-b}\left(1+\sqrt{\frac{T}{T_1}}\right)^{1+b}\right]^{-1} . \quad (18)$$

The parameters a, b, T_0, and T_1 are given in Table 1.

2.2. *CO Molecule*

For the carbon monoxide molecule, we consider one formation process (radiative association) and three destruction processes: thermal destruction due to interactions with the surrounding gas in thermodynamic equilibrium, non-thermal destruction due to collisions with Compton electrons, and destruction due to the reaction with a He^+ cation. The formation rate was computed using an analytic interpolation of the tabulated data of Dalgarno et al. (1990):

$${}^{+}k_{\rm CO} = \frac{4.467\times10^{-17}}{\sqrt{\left(\frac{T}{4467}\right)^{-2.08}+\left(\frac{T}{4467}\right)^{-0.22}}} \quad (19)$$

In the absence of non-thermal electrons, the concentration of the CO molecule is given by (e.g., Clayton 2013):

$$n_{\rm CO} = n_{\rm C} n_{\rm O}\left(\frac{h^2}{2\pi MkT}\right)^{3/2} e^{\frac{B_{\rm CO}}{kT}} \quad (20)$$

where h is Planck's constant, k is Boltzmann's constant, M is the reduced mass of C and O, and $B_{\rm CO} = 11.1$ eV is the binding energy of the CO molecule. At equilibrium,

$$\frac{dn_{\rm CO}}{dt} = 0 = {}^{+}k_{\rm CO} n_{\rm C} n_{\rm O} - {}^{-}k_{\rm CO} n_{\rm CO} \quad (21)$$

where ${}^{-}k_{\rm CO}$ is the thermal destruction rate of CO. This yields

$${}^{-}k_{\rm CO} = \frac{{}^{+}k_{\rm CO} n_{\rm C} n_{\rm O}}{n_{\rm CO}} = {}^{+}k_{\rm CO}\left(\frac{h^2}{2\pi MkT}\right)^{-3/2} e^{-\frac{B_{\rm CO}}{kT}} . \quad (22)$$

Note that we do not compute the CO abundance at equilibrium. We only assume, throughout this calculation, that the thermal destruction coefficient of the CO molecule is independent on the density of the molecule and therefore the destruction coefficient at equilibrium is the same as the coefficient out of equilibrium. A somewhat different value was obtained experimentally by Appleton et al. (1970), and used by Cherchneff & Dwek (2009, 2010). The Appleton et al. (1970) experiment, however, was carried out at much higher temperature (8000 − 15000 K) and may not be precise in the temperature range considered here.

The rate of CO molecule destruction due to interaction with non-thermal electron was computed with Equations 13, 14, and 15 adopting (Liu & Dalgarno 1995):

$$W_{\rm CO} = 125\,{\rm eV} \quad (23)$$

Finally, the CO destruction rate by interactions with He^+ cations was computed from the Arrhenius coefficient reported in the Umist Database for Astrochemistry 2012 (McElroy et al. 2013; `www.udfa.net`):

$${}^{-}k_{\rm CO,He^+} = 1.6\times10^{-9} \quad (24)$$

2.3. *Dust nucleation and growth*

The nucleation of stable carbonaceous grains is modeled following the kinetic theory of dust nucleation (Becker & Döring 1935; Kashchiev 2000), assuming local-thermal equilibrium and adopting the capillary approximation for clusters with more than two carbon atoms. The kinetic theory of dust nucleation describes the nucleation process as the result of a competition between attachment and detachment of carbon atoms to and from existing, unstable molecular clusters. The nucleation rate is given by the master equation,

$$J = n_{C,gas} f_1\left[1+\sum_{i=2}^{\infty}\left(\prod_{j=2}^{i}\frac{g_i}{f_i}\right)\right]^{-1} , \quad (25)$$

in which $n_{\rm C,gas}$ is the number density of carbon in the gas phase, f_1 is the rate of the $C + C \rightarrow C_2$ formation reaction, f_i is the rate of the $C_i + C \rightarrow C_{i+1}$ growth process, and g_i is the rate of the $C_i \rightarrow C_{i-1} + C$ detachment process.

The growth rate of the i-sized cluster, f_i, is taken to be the fraction λ of the impingement rate of gas phase carbon atom onto the cluster. The impingement rate can be derived from the kinetic theory of gases yielding a growth rate:

$$f_i = \lambda\, n_{\rm C,gas}\, c_{\rm s}\, (i\, v_{\rm C})^{2/3}\sqrt{\frac{kT}{2\pi m_{\rm C}}} \quad (26)$$

where $v_{\rm C} = 8.933\times10^{-24}\,{\rm cm}^3$ is the volume occupied by a carbon molecule in the solid phase, $m_{\rm C} = 2\times10^{-23}$ g is the mass of a carbon atom, and $c_{\rm s} = S/V^{2/3}$ the shape factor (S being the grain surface and V its volume). Analogously to previous work on dust formation in core-collapse supernova explosions, we assume throughout this paper $\lambda = 1$ and $c_{\rm s} = (36\pi)^{1/3}$, the shape factor of spherical grains. For a test on how assuming different values for these parameters affects the amount and timing of dust condensation, see Fallest et al. (2013).

A dedicated discussion is required for the formation of a dicarbon molecule from two C atoms. When a C atom approaches a C_i carbon cluster and binds to it, the excess energy is dissipated through an increase in the cluster temperature, distributed among its $3i-6$ vibrational degrees of freedom. This allows for non-radiative associations with a sticking coefficient of order unity. The same, however, cannot be said for the dimer formation. A dimer only has one vibrational degree of freedom and, should all the excess energy be dumped there, it would be large enough to break the bond and return the two C molecules to the gas phase. For this reason, instead of taking the limit $i = 1$ of Eq. 26, we adopt the C_2 formation rate from radiative association (Andreazza & Singh 1997):

$$f_1 = 4.36\times10^{-18}\left(\frac{T}{300}\right)^{0.35} e^{-\frac{161.31}{T}} n_{\rm C,gas} \quad (27)$$

A comparison between this rate and the rate obtained by using $i = 1$ in Eq. 26 is shown in Figure 1 as a function of temperature. The striking difference of many orders of magnitude between the two curves is a warning flag of how inadequate are some assumptions currently made in dust condensation

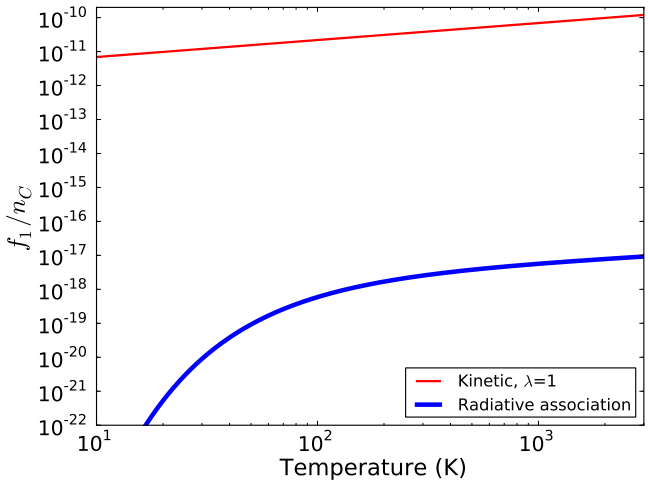


FIG. 1.— Comparison between the density normalized attachment rate of C atoms on C atoms to form a dicarbon molecule. The thick blue line shows the radiative association rate (from Andreazza and Singh 1997) that is used in this work. The thin red line shows the limit $i = 1$ of Eq. 26, implicitly adopted in most dust nucleation studies.

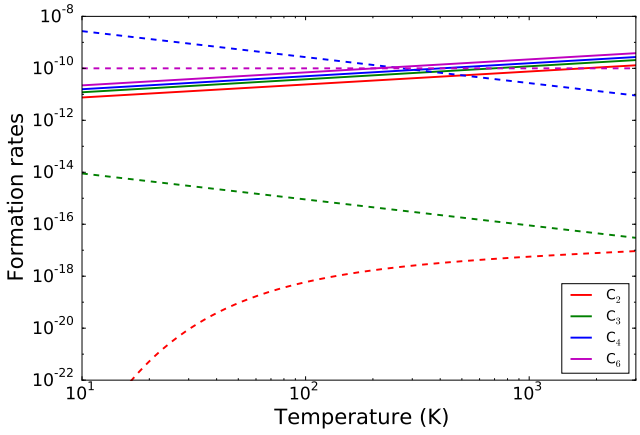


FIG. 2.— Comparison between the formation rate of carbon clusters of different size by monomer accretion as computed by radiative association (dashed lines) and by the nucleation theory (solid lines). In this paper we adopt the rates from the nucleation theory for any cluster with more than two atoms. See the text for a discussion.

calculations[6] (see also Donn & Nuth 1985). What happens for the formation of the C_i molecules with $i = 3, 4, 5$, and up to a few tens is not fully understood. Rates for radiative association have been computed by Wakelam et al. (2009) for a few carbon clusters (C_3, C_4, C_6, and C_8). Their results are compared to the nucleation theory rates in Figure 2. The difference between the nucleation and radiative association rates is, again, quite large. For the formation of clusters with more than two atoms, the reaction can be radiative or non-radiative, as assumed in the nucleation theory, since the extra energy of the incoming monomer can be absorbed in the 3i-6 degrees of freedom of the accreting cluster. Given the lack of a robust and complete set of radiative reaction rates, we here perform our calculations with the rates from the nucleation theory, the solid lines in Figure 2, as derived from Eq. 26.

In the absence of harmless radiation and cations, the ejection rates g_i can be computed by enforcing detailed equilibrium in a canonical ensemble of carbon particles at saturation. In such an ensemble, true equilibrium can be achieved, and the distribution of the number of clusters of size i is given by the Boltzmann equation,

$$n_i \propto e^{\frac{\sigma_C S_i}{kT}} , \tag{28}$$

where σ_C is the surface energy of solid phase carbon and S_i the surface area of the i-sized cluster. Detailed equilibrium reads:

$$n_i g_i = n_{i-1} f_{i-1} \tag{29}$$

from which we find

$$g_{i,\rm th} = f_{i-1} e^{\frac{\sigma_C}{kT}(S_i - S_{i-1})} \simeq f_{i-1} e^{\frac{2\sigma_C c_s v_C^{2/3}}{3i^{1/3}kT}} = $$
$$= n_{C,\rm eq} \lambda c_s [(i-1) v_C]^{2/3} \sqrt{\frac{kT}{2\pi m_C}} e^{\frac{2\sigma_C c_s v_C^{2/3}}{3i^{1/3}kT}} \tag{30}$$

where the subscript $_{\rm th}$ indicates that the above detachment rate is the rate of spontaneous detachments from a cluster at temperature T. In the environment of a supernova remnant, additional processes can enhance the loss of monomers from clusters, and therefore increase the total ejection rate. In this work we consider the chemical reactions between helium cations and carbon clusters (ion-molecule) and the reaction between a carbon cluster and an oxygen atom to give a carbon monoxide molecule and a smaller cluster. Both reactions have been studied only with very small carbon clusters C_i with $i < 10$.

The reaction of carbon clusters with oxygen atoms was studied by Woon & Herbst (1996) and Terzieva & Herbst (1998) for carbon clusters up to 9 atoms (see also Cherchneff & Dwek 2010). They found that the reaction rate with i-sized clusters per unit time and volume $k_{(9),i}$ is given by:

$$k_{(9),i} = A_{(9),i} \left(\frac{T}{300}\right)^{b_{(9),i}} e^{-\frac{T_{(9),i}}{T}} n_{C_i} n_O \tag{31}$$

where the subscript of the coefficients of the modified Arrhenius equation refer to Eq. 9. Terzieva & Herbst (1998) find that the coefficients $A_{(9),i}$, $b_{(9),i}$, and $T_{(9),i}$ depend on the parity of the cluster size i but do not change monotonically with it. This is understood as a consequence of the fact that the most stable allotrope of C_i with $i \leq 9$ is a linear chain, with dangling bonds at the two extremities irrespective of the size. For $10 \leq i \leq 26$ carbon clusters organize in rings, while for bigger clusters they form closed three-dimensional structures (Mauney et al. 2015). In vacuum, big carbon clusters form fullerenes. It is believed that astrophysical carbonaceous grains are mainly in the form of amorphous carbon and/or graphite onions or flakes. Either case, it is reasonable to assume that the number of dangling bonds that can react with free oxygen atoms grows with the cluster surface. Under our assumption of spherical grains, we have therefore that the loss of carbon monomers from an i-sized cluster due to oxygen weathering is[7]:

$$g_{i,O} = 10^{-11} e^{-\frac{1130}{T}} n_{O,\rm gas} i^{2/3} , \tag{32}$$

where $n_{O,\rm gas}$ is the density of gas-phase oxygen atoms.

An analogous discussion holds for the ion-molecule reaction 10 whose Arrhenius coefficients for C_i clusters with

[6] An alternative path to the carbon dimer involves the formation of a CO molecule and its reaction with a free carbon atom. This was shown to be less effective by Yu et al. (2013).

[7] Adopting the approximation below or the computed values for the small carbon clusters with up to 10 atoms (Terzieva & Herbst 1998) does not result in any significant difference in the dust formation yields or carbon monoxide abundance. We show below the results from the approximation of Eq 32.

$i \leq 10$ are presented in the UMIST Database for Astrochemistry 2012 (McElroy et al. 2013). In this case the coefficients have no dependence on i, not even with parity. Again, we assume that the reaction rate is proportional to the number of dangling bonds which, in turn, scales with the grain surface. We have therefore that the loss of carbon monomers from an i-sized cluster due to HeII weathering is:

$$g_{i,\mathrm{He}} = 1.6 \times 10^{-9} n_{\mathrm{HeII}} i^{2/3} \tag{33}$$

where n_{HeII} is the density of singly ionized helium atoms.

The total ejection rate that we use in Eq. 25 is therefore the sum of the spontaneous ejection rate plus the chemical weathering due to oxygen and ionized helium:

$$g_i = g_{i,\mathrm{th}} + g_{i,\mathrm{O}}, + g_{i,\mathrm{He}} \tag{34}$$

The consequence of this equation is that the ejection rate is increased, making nucleation of new grains more difficult. The spontaneous ejection rate allows for nucleation as soon as the saturation is larger than one, and nucleation becomes efficient for saturation larger than a few. As we will see in the following, in the environment of a SNR chemical weathering of the forming grains is so efficient that nucleation only takes place for saturations of many orders of magnitude larger than unity.

No matter how hampered by chemical weathering, the nucleation of small grains still takes place, albeit at a much reduced rate. Once stable grains are formed (where stable means bigger than the critical size at which $f_i = g_i$, their size evolves according to the same accretion and decretion rate discussed above. Such critical size is a function of temperature and saturation and ranges between approximately 3 Å and 30 Å. The growth of existing grains of size i in monomers per second is regulated by the equation

$$\left.\frac{dn}{dt}\right|_i = f_i - g_i \,. \tag{35}$$

Note that the stability of grains can change as a result of the cooling of the gas (increasing stability) and of the decrease of gas-phase C atoms (decreasing stability) and therefore a grain that is formed as stable at some time can later become unstable and shrink in size.

3. SUPERNOVA MODEL

We simulated a $15\,\mathrm{M}_\odot$ solar model with initial solar composition of Lodders et al. (2009) from the zero-age main sequence to pre-SN phase using the KEPLER (Weaver et al. 1978) stellar evolution code. We use the same prescription of hydrodynamic instabilities (semiconvection, overshoot, convection mixing length parameter), nuclear reaction rates, and mass loss rates as in Woosley & Heger (2007). Figure 3 shows the Kippenhahn Diagram of the pre-supernova evolution, and Figure 4 the composition of the model at pre-supernova stage. We simulate the explosion using a hydrodynamic spherically symmetric piston that is adjusted to yield a total kinetic energy of the ejecta of 1.2×10^{51} erg (see Rauscher et al. 2002 for a more detailed description). The post-SN mixing due to Rayleigh-Taylor instabilities is approximated by a simple "boxcar" model and adjusted to mix ^{56}Ni out into the envelope such that typical SN light curves are reasonably reproduced (Figure 5, see also Rauscher et al. 2002). The amount of mixing is consistent with hydrodynamic simulations (e.g., Joggerst et al. 2010).

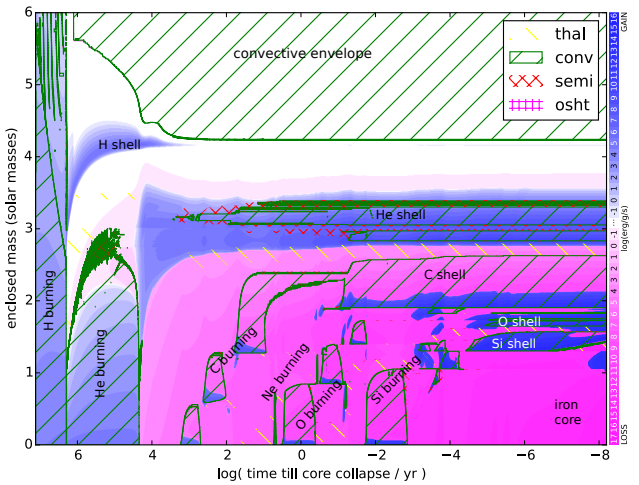


FIG. 3.— Kippenhahn diagram of the pre-supernova evolution of the **inner $6\,\mathrm{M}_\odot$ of a $15\,\mathrm{M}_\odot$** progenitor star. The *x-axis* shoes the time till core collapse in yr, from 30 million yr before collapse to 250 ms before core bounce; the *y-axis* is the mass coordinate; *blue shading* indicate regions where nuclear energy generation exceeds neutrino losses, *purple shading* where neutrino losses dominate; *green hatching* (framed) indicates convective regions, *horizontal/vertical purple hatching* indicates convective overshooting (not visible), *red cross hatching* indicates semi-convective regions, and *yellow hatching* thermohaline mixing. **Major nuclear burning stages are indicated.**

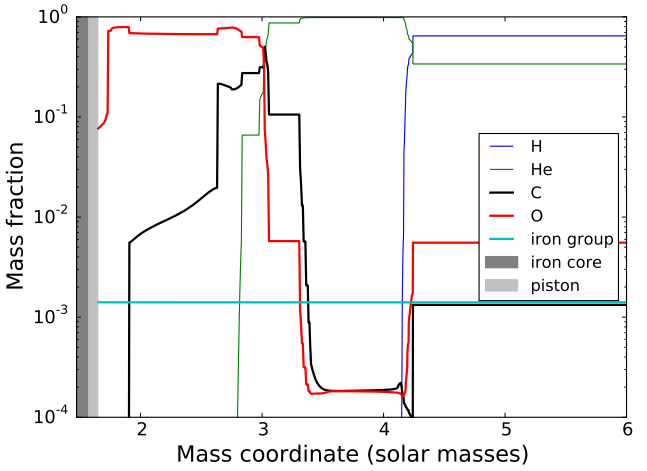


FIG. 4.— Presupernova structure of the $15\,\mathrm{M}_\odot$ model. *Dark gray shading* indicates the iron core and *light gray shading* the location of the piston (initial mass cut). **The mass coordinate has been truncated on both sides. The envelope is chemically homogeneous above $6\,\mathrm{M}_\odot$ and the total mass of the star at the time of supernova is $11.185\,\mathrm{M}_\odot$.**

Note that the ^{56}Ni present in the innermost layers seen in Figure 6 is made in the supernova explosion by shock heating. The ^{4}He seen in this region is due to photo-disintegration by the shock and incomplete recombination to ^{56}Ni. For reference, this is the same $15\,\mathrm{M}_\odot$ model also included in Patnaude et al. (2015).

4. RESULTS

In this section we present the results of our calculations focusing on the differences between results from the carbon nucleation, growth and weathering presented here with respect to more traditional calculations based on classical nucleation theory and alternative approaches that aim at taking into account the chemistry involved in the formation of the small dust seeds. Let us first look in detail at the temporal evolu-

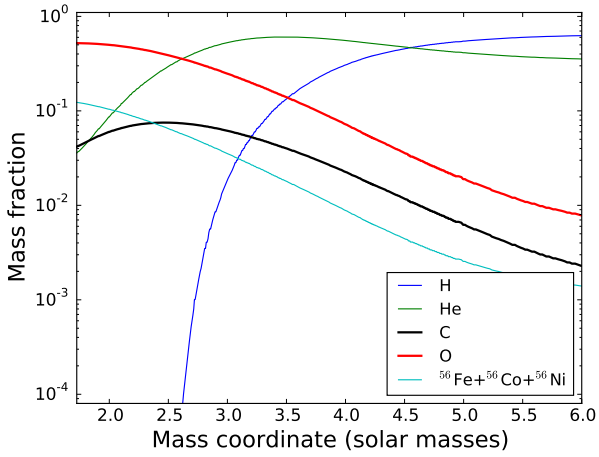


FIG. 5.— Post-explosion mass fraction of the elements relevant to carbonaceous dust formation as a function of the inner enclosed mass for the mixed stellar progenitor.

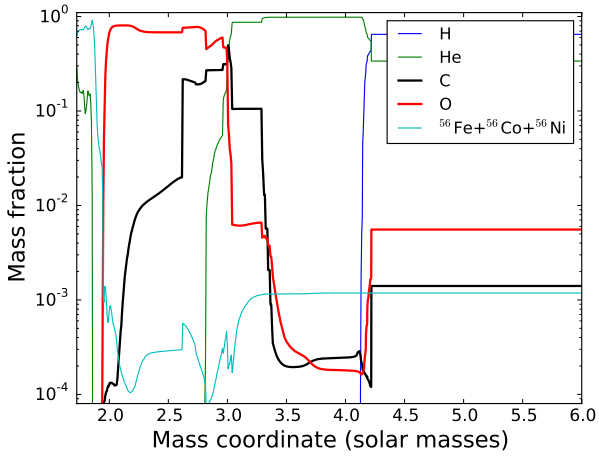


FIG. 6.— Same as Figure 5 but for the unmixed model.

TABLE 2
PROPERTIES OF REPRESENTATIVE ZONES.

Zone Name	Zone #	Mass Coordinate (Solar Masses)	n_C/n_O mixed	n_C/n_O unmixed
A	69	2.11	0.18	0.0016
B	209	3.0	0.22	1.44
C	556	5.0	0.44	0.32

[a] logarithm base 10 of number ratio

tion of the properties of a few representative single shells. We chose three representative shells zones (Table 2) in the unmixed stellar progenitor model (Figure 6). Zone A is located at the $2\,M_\odot$ mass coordinate, and is characterized by a marked oxygen overabundance with respect to carbon (approximately three orders of magnitude). Zone B is located at mass coordinate $3\,M_\odot$ and has approximately equal abundances of C and O. It is also the most carbon-rich zone in the whole ejecta. Finally, Zone C is located at mass coordinate $5\,M_\odot$ well outside the region were explosive nucleosynthesis was active. It is characterized by an overabundance of O by a factor ~ 3 with respect to C. The thickness of each zone is small and within each of them the densities and thermodynamic properties are

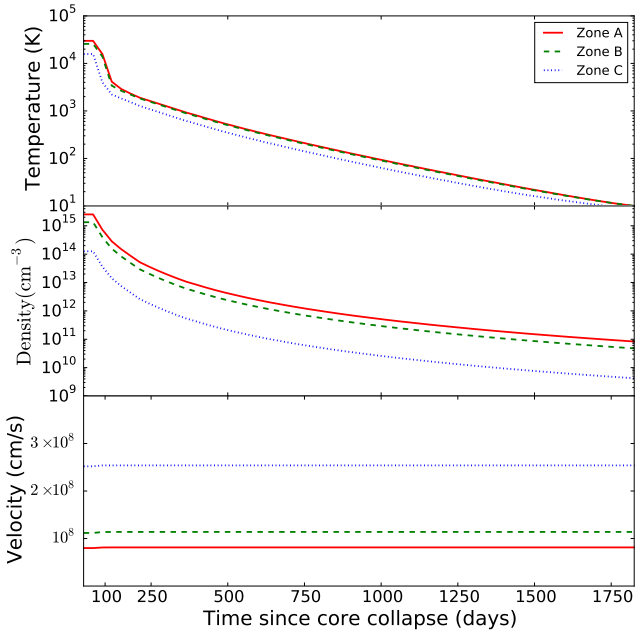


FIG. 7.— Temporal evolution of the dynamical properties of the three zones for which the dust formation and chemical evolution is discussed in more detail in the text. See Table 2 for more details on the three zones.

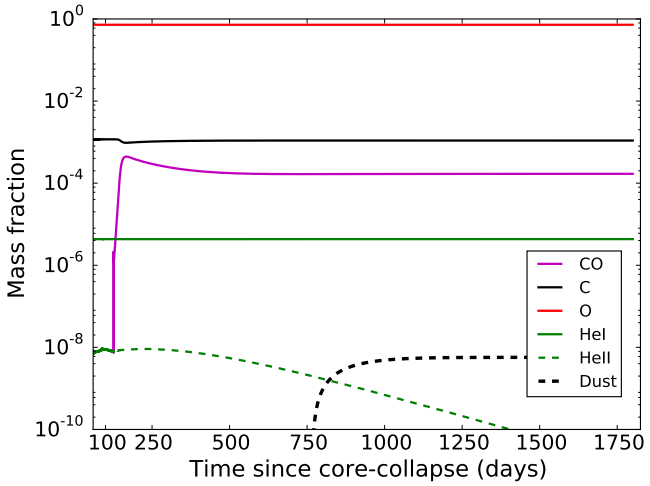


FIG. 8.— Mass fraction of relevant species (atoms, ions, molecules, or dust) as a function of time in the Simulation Zone A (Table 2).

constant at any given time. The dynamical evolution of the three zones (temperature, density, and expansion velocity) is shown in Figure 7.

Figures 8, 9, and 10 show the temporal evolution of the ejecta composition in the three selected zones for the unmixed progenitor model. Despite some differences, all the plots show some important common features. First, the formation of the CO molecule is never efficient enough to completely absorb all the carbon, even in Zone A, where oxygen is largely overabundant with respect to carbon (see analogous results by Clayton et al. 2001; Deneault et al. 2006, and Clayton 2013). Second, a sizable fraction of He is ionized to the He^+ cation, and its weathering effect can delay dust formation. This is particularly clear in Zone B, where dust initially forms quickly at $t \sim 7$ months after the explosion. The He^+ concentration, however, peaks a few months later causing a temporary decrease in the dust fraction. Eventually, the ion-

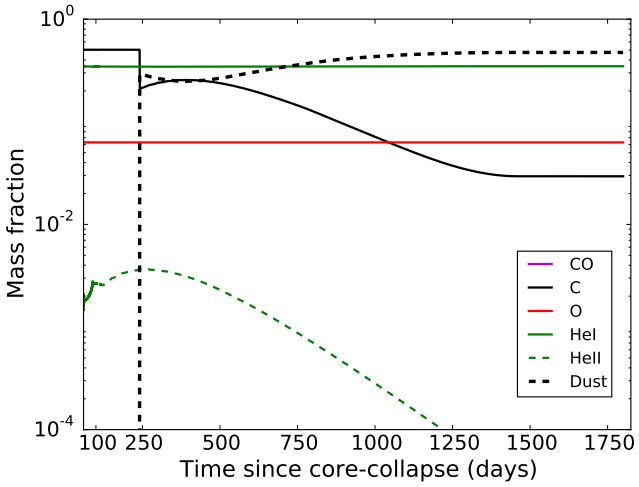


FIG. 9.— Same as Figure 8 but for Zone B (Table 2).

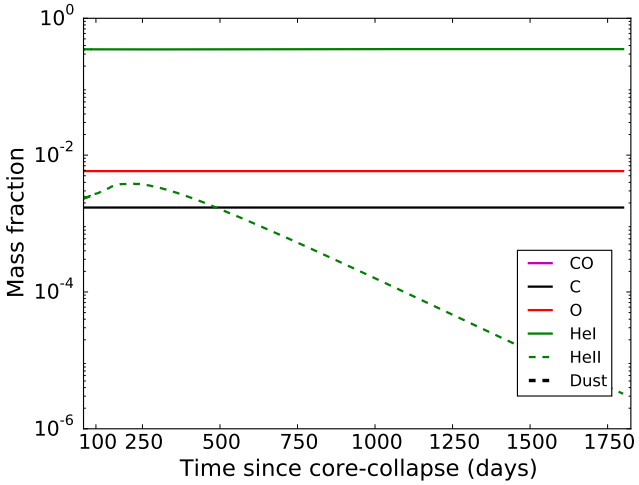


FIG. 10.— Same as Figure 8 but for Zone C (Table 2).

ized He fraction drops again and dust nucleation and growth resume. This result not only shows the important effects of weathering in the supernova environment, it also shows that the customary assumption that once a grain has grown beyond the critical size it only grows further is inaccurate. Weathering can become dominant and shrink or completely destroy the already formed grains. Oxidation is also important in limiting the dust formation and growth. Its effect, however, is less clear in the figures because the O abundance is constant with time. The rate of the He-C_i ion-molecule reaction is also approximately two orders of magnitude faster than the oxidation reaction, making the cation the most damaging weathering agent in all regions except for those in which oxygen is particularly abundant.

Figures 8, 9, and 10 also show that the dust condensation time and its efficiency vary significantly across the remnant. Condensation is significantly delayed in the inner mass coordinate, starting only $\sim$2 years after core-collapse. Mostly due to atomic carbon depletion into CO, the dust condensation efficiency is very small in Zone A. In the carbon-rich area of Zone B, instead, dust formation sets in early, but is subsequently reversed into dust destruction by the increasing ionization of helium. Only a few years after core collapse dust formation reaches its final efficiency, almost 100%. Finally, no dust is formed in the outer layers of the star (Zone C).

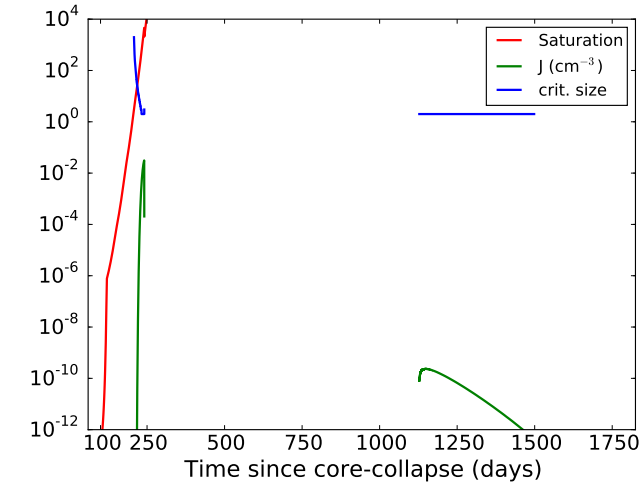


FIG. 11.— Evolution of the saturation (S), nucleation rate (J) and critical size of Zone B (Table 2).

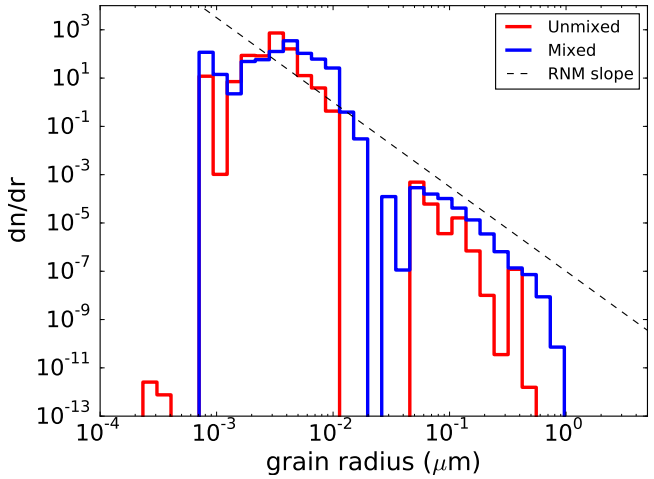


FIG. 12.— Size distribution of the carbon grains for the Mixed and Unmixed models integrated over the whole ejecta at 60 months after core-collapse.

A fundamental role in altering the nucleation pattern of carbonaceous dust is also played by the difficulty in forming the dimer, as discussed above. Figure 11 shows the saturation, nucleation rate, and critical size of the forming carbon grains as a function of time for Zone B. We first note that saturation does not play the same role that it does in the thermodynamic theory of homogeneous nucleation. In that case, the solid phase is expected to start nucleating as soon as saturation grows above a few. In our calculation, saturation can grow to extremely high values, as large as a double precision real number can handle. Yet, nucleation proceeds slowly, and can even be turned off while the saturation is increasing. What we see in the figure is that initially, as saturation becomes larger than one, a spike of nucleation is observed (at $t \sim 7$ months). During this phase the spontaneous ejection of monomers from unstable carbon clusters dominates over the oxidation and charge-exchange rates. As usual, in this phase the growth of the saturation produces an increased nucleation rate and smaller critical size. Differently from classical calculations, however, our nucleation rate is limited by the dimer formation rate (Eq. 27).

As time progresses, the concentration of HeII cations in-

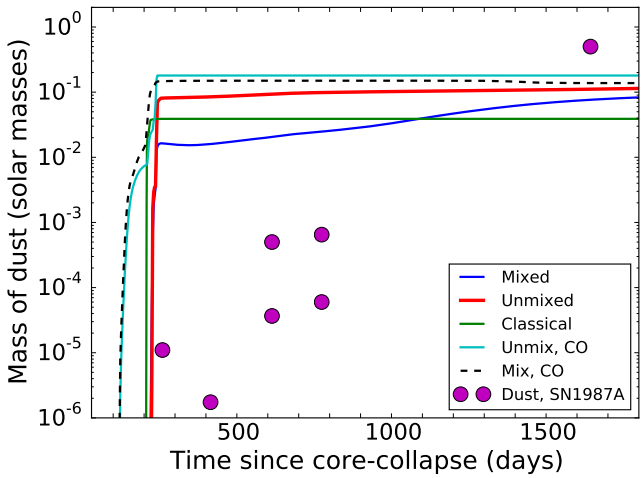


FIG. 13.— Evolution of the total mass of carbonaceous grains since the core-collapse. Various dust formation models are used and are shown in different colors, as discussed in the text.

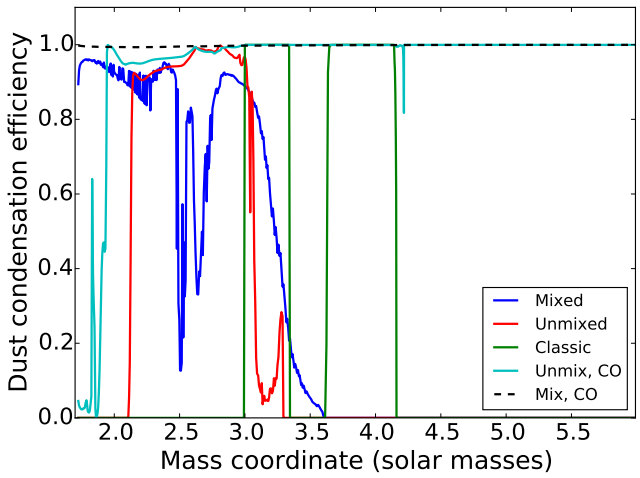


FIG. 14.— Efficiency of the carbonaceous dust condensation at Year 5 (the last time of our simulations) as a function of the mass coordinate. The efficiency is defined as the mass in dust grains over the total carbon mass.

creases and the charge-exchange weathering process becomes dominant, shutting off entirely the nucleation of new grains and shrinking the already existing ones (see the decreasing dust mass fraction between ~ 7 and ~ 13 months in Figure 9). In this period, the saturation becomes virtually infinite. Yet, nucleation is entirely shut off because the weathering rate is larger than the accretion rate of carbon atoms on any size grain. At later times ($t > 35$ months) the charge-exchange weathering still dominates the ejection rate, but the accretion of carbon atoms now dominates the rates. Nucleation can therefore proceed, with a formal critical size of two atoms. Again, the nucleation rate is constrained by the rate of the formation of the dimer. The plots for the other two zones are analogous, but with only a subset of the phenomenology of what seen in Zone B. The inner Zone A does not have enough carbon to trigger the initial burst of dust formation, and nucleation is postponed until $t \sim 2$ years, when the ion-molecule weathering rate becomes smaller than the accretion rate. The nucleation takes place very slowly, being limited by the rate of dimer formation. For the outer Zone C, instead, nucleation never takes place, because the carbon abundance is so low compared to the He abundance that charge-exchange weathering is always dominating over the growth of carbon clusters.

Let us now look at nucleation and growth of carbonaceous dust in the whole ejecta. Figure 12 shows the comparison of the final grain size distributions at 5 years past the core collapse for the mixed and unmixed models. Both distributions have been normalized to unit integral to facilitate the comparison and a dashed line has been added to show the classical MRN interstellar size distribution (Mathis et al. 1977). In both cases we obtain a broad size distribution that is somewhat steeper than the MRN distribution. The Mixed progenitor model gives a bigger upper limit for the grain size. Since the gain population still needs to cross the reverse shock, where the smallest grains are likely to be destroyed by sputtering (Nozawa et al. 2006; Bianchi & Schneider 2007), the small differences seen here could be much more substantial when the dust is recycled into the interstellar medium.

In the following, we consider a suite of codes with different assumptions to compare and understand the effect of adding new processes in the dust formation process. The first code, which is labeled as "Classical" in the figures, adopts the stan-

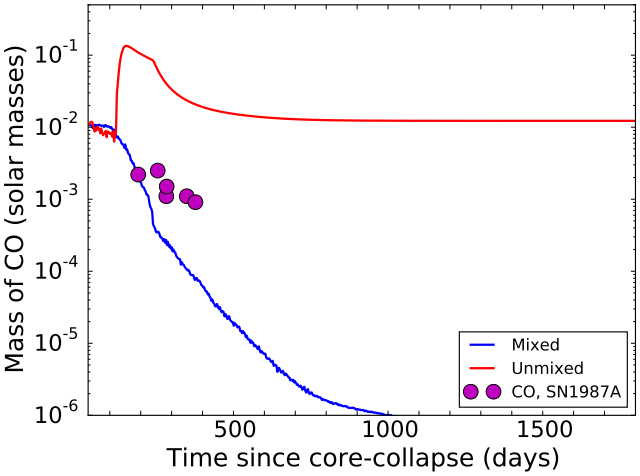


FIG. 15.— Evolution of the total mass of CO as a function of time since the core-collapse. The various models are shown in different colors, as discussed in the text.

dard assumptions of classical calculations. In this version of the code, nucleation takes place only in regions where the number density of carbon atoms is larger than that of oxygen atoms. The nucleation rate is computed according to the thermodynamic theory as (e.g., Fallest et al. 2011 and references therein):

$$J = \left(\frac{c_s^3 v_C^2 \sigma}{18\pi^2 m_C}\right)^{1/2} n_C^2 \, e^{-\frac{4c_s^3 v_C^2 \sigma^3}{27(kT)^3(\ln S)^2}} \qquad (36)$$

where we adopt the value $\sigma = 1500\,\mathrm{dyne/cm}$ for the amorphous carbon surface energy. Within this theory, the critical grain size can be found analytically as

$$n^* = \frac{8c_s^3 v_C^2 \sigma^3}{27(kT \ln S)^3} \qquad (37)$$

This dust model was applied only to the unmixed progenitor, since the mixed one does not have any zone in which $n_C > n_O$.

The second model we adopt is a slight modification of the "Classical" one, in which the formation and destruction of the CO is followed as described in Sect. 2.2. This allows for the formation of carbonaceous dust even in regions with $n_C \leq n_O$,

and therefore the model is run on both our mixed and unmixed progenitor models. The results are labeled in the figures as "Unmix, CO" and "Mix, CO". Finally, our full code described in Sect. 2 was applied to both the mixed and unmixed progenitor models. The results are labeled in the figures as just "Mixed" and "Unmixed".

Figure 13 shows the time evolution of the total mass condensed in carbonaceous grains. As expected, we see that all models based on classical nucleation have a sharp rise in the dust mass, due to a catastrophic dust formation event at about 7 months after core collapse. The dust mass is subsequently constant. This is in strong contrast with the continuum dust condensation detected in a sample of CCSN (Gall et al. 2014) and shown with the magenta symbols that represent dust detections in the remnant of SN1987A (Wooden et al. 1993; Ercolano et al. 2007; Matsuura et al. 2013; Indebetouw et al. 2014). The "Mixed" and "Unmixed" models, instead, show a more continuous formation of dust, starting approximately at 7 months (as for the classical models). Yet, even the more progressive dust formation of the Mixed and Unmixed models including weathering is still too fast to fully reproduce the observations. Dust formation in our simulations is continuously active for at least 5 years after core collapse, after which our calculations were halted. Extending the calculations for longer times is possible but not simple, since the thermal balance of the remnant becomes much more complex. Condensation is not expected to proceed much further, however, since in all the dust formation zones most of the available carbon has already been used by Year 5. This is shown in Figure 14, where the efficiency is plotted for the various models as a function of the mass coordinate. Efficiency here is defined as the ratio of the mass of carbon in grains over the total mass of carbon. Where dust formation takes place, it is almost inevitably highly efficient (~ 1), converting the vast majority of carbon into solid grains. This is not a trivial result. Consider, for example, model "Mix, CO". In all the zones oxygen is overabundant with respect to carbon. One might think, therefore, that most of the carbon should remain locked in CO molecules instead of condensing in carbonaceous grains. Instead, we see that while the CO molecule does form, it is continuously dissociated by Compton electrons. Grains instead, once they have managed to grow beyond a certain size, are much more resilient due to the fact that only the surface can be weathered by oxidation and ion-molecule reactions. In addition, Compton electrons are not damaging to grains because of the huge mass difference. Classical models with CO formation/dissociation, therefore, have virtually 100 % condensation efficiency of all carbon into grains across the entire star. The classical model without CO dissociation, instead, has 100 % efficiency but only in those zones where $n_{\rm C} > n_{\rm O}$.

The behavior of the complete models is more complex. Dust condensation takes place only in the inner part of the star, within about 3.5 solar masses from the center. In this case, the reason for the lack of condensation at large distances from the center of the star is the large number of He cations that erode the carbon clusters before they can reach a size large enough to become self-shielded. By the time the radioactivity has ceased and the He^+ fraction decreases, the gas is too diffuse and cold for efficient nucleation. Yet, as discussed above, efficiency is large where condensation takes place, almost always exceeding 50 %, and therefore we do not expect to see much dust mass growth beyond the five years of the computation. Figure 15 shows instead the mass of CO in the entire remnant for the various models (except the classical model, for which the CO molecule is not considered) as a function of time. Theoretical predictions are compared against the measurement of CO in the remnant of SN1987A (Spyromilio et al. 1988). Also in this case the theoretical predictions are in qualitative agreement with the data, the Mixed model performing better than the unmixed one. Detailed agreement is not expected since the CCSN progenitor model is not designed to closely reproduce the progenitor of SN1987A. Figure 16 shows the condensation times of the grains as a function of the mass coordinate. Here we define the condensation time as the time at which half of the local carbon is converted into grains. The classical models, again, show the lowest diversity, with dust forming at about seven months at all distances. The complete models show instead a distance dependent condensation history. The mixed model, owing to it smoother profile of abundances, has a somewhat monotonic dependence with the earliest formation just outside of the stellar core, and progressively longer formation times out to a mass coordinate of $\sim 3.2\,{\rm M}_\odot$ where the efficiency drops below 50 % and the condensation time is no longer well-defined. The unmixed model has instead a more diverse behavior affected by both the sharp composition changes and the dust formation physics. Either way, different condensation times at different radii are the cause of the more progressive dust formation history seen in Figure 13 for the complete models.

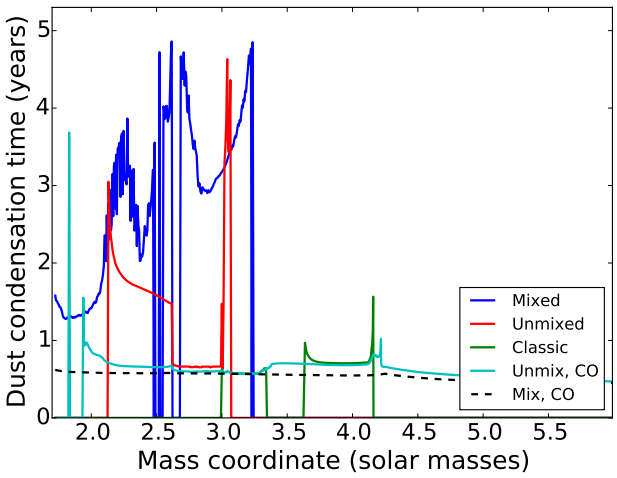


FIG. 16.— Condensation time as a function of the mass coordinate (which is monotonically related to the distance from the center of the explosion). The condensation time is defined as the time at which 50 % of the total carbon is condensed into grains.

Finally, Figure 17 shows the average grain size in each zone at the end of the calculation. None of the models has a clearly understandable pattern, with the exception of the complete mixed model, for which the biggest grains are formed close to the core. Grains that form earlier have more time to grow and therefore are eventually bigger. The average size, however, depends also on the rate at which nucleation takes place, and from the speed at which carbon initially locked into CO molecules is released for use in dust condensation.

5. SUMMARY AND DISCUSSION

We have presented a calculation of carbonaceous dust formation in a $15\,{\rm M}_\odot$ progenitor star exploding as a core-collapse supernova. Our study is based on a novel nucleation code that was developed to address the particular conditions of the exploding supernova. This is a rapidly evolving environment with plenty of ionizing radiation and reactive agents

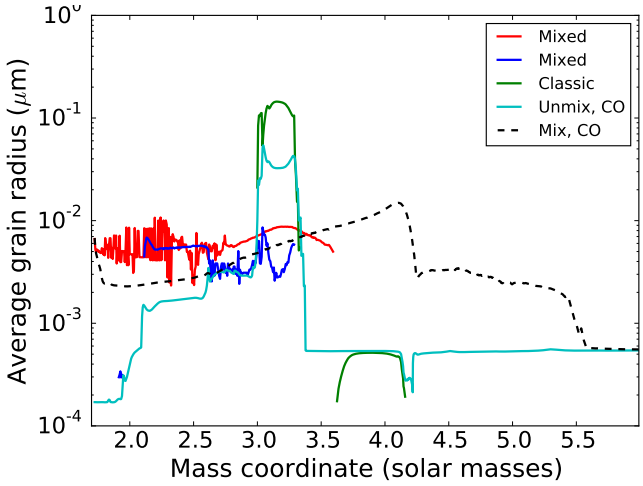


FIG. 17.— Average dust grain size at 5 years post core collapse as a function of the mass coordinate for the various dust condensation models.

that can harm the forming grains. Our code uses the kinetic theory of nucleation in order to be suitable for possible non-steady state conditions in the fast evolving remnant. In addition, the flexibility of the kinetic theory allows us to relax the capillary approximation for the dimer (C_2) formation and to include the effect of oxidation and ion-molecule reactions in the calculation. An alternative framework for joining the chemical and nucleation approaches has been recently presented by Sarangi & Cherchneff (2015). Their approach differs fundamentally from what presented in this paper in that the chemical phase is joined to a coalescence phase, rather than to a growth phase. This means that in their scheme carbon clusters form up to a maximum size of ten atoms until all the carbon gas has been used and subsequently grow by coagulation with other clusters rather than grow by adsorption of gas monomers (or molecules). We find that, at least for carbon, the chance of collisions of molecular clusters with monomers is far larger than with other clusters. In our calculations monomers are more abundant than clusters and, being lighter, have a larger thermal velocity that makes collisions more frequent. As a subsequent step in understanding nucleation, however, the coagulation and growth should be integrated and taken into account simultaneously.

With respect to classical calculations (Kozasa et al. 1989, 1991; Todini & Ferrara 2001; Nozawa et al. 2003; Fallest et al. 2011) and to the results of Sarangi & Cherchneff (2015), we find that our new code predicts a much more gradual carbon dust formation, beginning just a few months after the core collapse and continuing for a few years. Despite the more gradual formation, however, we are not able to fully reproduce the observational results that require an even more gradual and continuous dust formation in the ejecta, with dust appearing as early as two months after core collapse and gradually increasing for a few years to a decade (Gall et al. 2014) eventually leading to a highly efficient condensation of a sizable fraction of a solar mass (Indebetouw et al. 2014). Addition of non-carbonaceous dust chemistry (e.g., Sarangi & Cherchneff 2015) and/or a fully three-dimensional calculation (Lazzati & Fallest, in preparation) can ameliorate the discrepancy. It must be also noted that the explosion model plays a role in the grain formation. A less energetic explosion than the one we used (or one with more massive ejecta) would result in higher densities and temperatures at long timescales, allowing for a longer period of growth and, potentially, more dust condensation. On the other hand, a more energetic explosion or one with lighter ejecta would result in colder and less dense gas, likely going earlier into freeze-out. The role of explosion diversity is certainly as important as the proper dimensionality of the simulation, since a 3D model is likely going to contain both faster and slower ejecta than the 1D spherically simmetric model presented here and elswhere in the literature.

Even though we consider this work a step forward towards a complete understanding of dust formation in stellar explosions (and in general), it is still plagued by some serious limitations. The most obvious is the fact that we consider only carbonaceous dust, while more species are known to condensate in supernova explosions. Condensation of silicates and other dust species can begin earlier and explain the early dust formation observed in some SNe (Wooden et al. 1993; Gall et al. 2014; Sarangi & Cherchneff 2015). On a more fundamental level, our code still assumes a constant sticking coefficient $\lambda = 1$, a spherical shape for the forming grains, down to the smallest sizes, and the capillary approximation of a size-independent surface energy for any cluster with $i > 2$. All these are important limitations that need to be corrected (see, e.g., Mauney & Lazzati 2015) before a serious comparison with data can be performed. As any nucleation based work, we also assume that grain formation and growth takes place by addition of single carbon atoms, and that grain erosion as well takes place by removing one atom at a time from a cluster. Reactions that cause the splitting of a cluster in two fragments are not considered, even though they might be important, especially at low temperature (see, e.g., Wakelam et al. 2009). Another important issue is whether the chemical and nucleation approaches are fully consistent with each other. As we show in Fig. 2, that might not be the case, creating a serious issue when they are joined. More theoretical and experimental work needs to be devoted to understanding the formation rates of carbon clusters with a few up to a few tens of atoms, and the relative importance of radiative and non-radiative association processes need to be pinned down from first principles. The reaction network is also incomplete, lacking the consideration of the effect of other potentially harmful cations, such as Ar^+ and Ne^+. The role of these cations in silicate nucleation and growth was included in the work of Sarangi & Cherchneff (2013, 2015), but ion-molecule reaction rates for such cations with carbon clusters are not available in the literature and are therefore omitted in this work.

We are very grateful to the anonymous referee for her/his useful and constructive comments. This work was supported in part by NSF grants AST-1150365 and AST-1461362 (DL), and by an ARC Future Fellowship FT120100363 (AH).

REFERENCES

Andreazza, C. M., & Singh, P. D. 1997, MNRAS, 287, 287
Becker, R., & Döring, W. 1935, Ann. Phys. (Leipzig) 24, 719
Beelen, A., Cox, P., Benford, D. J., et al. 2006, ApJ, 642, 694
Bertoldi, F., Carilli, C. L., Cox, P., et al. 2003, A&A, 406, L55
Bianchi, S., & Schneider, R. 2007, MNRAS, 378, 973
Biscaro, C., & Cherchneff, I. 2014, A&A, 564, A25
Cherchneff, I., & Lilly, S. 2008, ApJ, 683, L123
Cherchneff, I., & Dwek, E. 2009, ApJ, 703, 642

Cherchneff, I., & Dwek, E. 2010, ApJ, 713, 1
Clayton, D. D., Deneault, E. A.-N., & Meyer, B. S. 2001, ApJ, 562, 480
Clayton, D. D. 2013, ApJ, 762, 5
Dalgarno, A., Du, M. L., & You, J. H. 1990, ApJ, 349, 675
Dalgarno, A., Yan, M., & Liu, W. 1999, ApJS, 125, 237
Deneault, E. A.-N., Clayton, D. D., & Meyer, B. S. 2006, ApJ, 638, 234
Donn, B., & Nuth, J. A. 1985, ApJ, 288, 187
Ercolano, B., Barlow, M. J., & Sugerman, B. E. K. 2007, MNRAS, 375, 753
Fallest, D. W., Nozawa, T., Nomoto, K., et al. 2011, MNRAS, 418, 571
Feder, J., Russell, K. C., Lothe, J., & Pound, G. M. 1966, Advances in Physics, 15, 111
Gall, C., Hjorth, J., Watson, D., et al. 2014, Nature, 511, 326
Indebetouw, R., Matsuura, M., Dwek, E., et al. 2014, ApJ, 782, L2
Joggerst, C. C., Almgren, A., Bell, J., Heger, A., Whalen, D., Woosley, S. E. 2010, ApJ, 709, 11
Kashchiev D., 2000, Nucleation: Basic Theory With Applications. Butterworth-Heinemann, Oxford
Kozasa, T., Hasegawa, H., & Nomoto, K. 1989, ApJ, 344, 325
Kozasa, T., Hasegawa, H., & Nomoto, K. 1991, A&A, 249, 474
Liu, W., & Victor, G. A. 1994, ApJ, 435, 909
Liu, W., & Dalgarno, A. 1995, ApJ, 454, 472
Lodders, K, Palme, H., Gail, H.-P. 2009, In Landolt- Börnstein, New Series, Vol. VI/4B, Chap. 4.4, J.E. Trümper (ed.), Berlin, Heidelberg, New York: Springer-Verlag, p. 560-630; arXiv:0901.1149v2
Maiolino, R., Schneider, R., Oliva, E., et al. 2004, Nature, 431, 533
Mathis, J. S., Rumpl, W., & Nordsieck, K. H. 1977, ApJ, 217, 425
Matsuura, M., Dwek, E., Meixner, M., et al. 2011, Science, 333, 1258
Mauney, C., Buongiorno Nardelli, M., Lazzati, D. 2015, ApJ, 800, 30
McElroy, D., Walsh, C., Markwick, A. J., et al. 2013, A&A, 550, A36
Nozawa, T., Kozasa, T., Umeda, H., Maeda, K., & Nomoto, K. 2003, ApJ, 598, 785
Nozawa, T., Kozasa, T., & Habe, A. 2006, ApJ, 648, 435
Nozawa, T., Kozasa, T., Tominaga, N., et al. 2010, ApJ, 713, 356
Patnaude, D. J., Lee, S.-H., Slane, P. O. , Badenes, C., Heger, A. , Ellison, D. C., Nagataki, S. 2015, ApJ, in press.
Priddey, R. S., Isaak, K. G., McMahon, R. G., Robson, E. I., & Pearson, C. P. 2003, MNRAS, 344, L74
Rauscher, T., Heger, A., Hoffman, R. D., Woosley, S. E. 2002, ApJ, 576, 323
Robson, I., Priddey, R. S., Isaak, K. G., & McMahon, R. G. 2004, MNRAS, 351, L29
Sarangi, A., & Cherchneff, I. 2013, ApJ, 776, 107
Spyromilio, J., Meikle, W. P. S., Learner, R. C. M., & Allen, D. A. 1988, Nature, 334, 327
Szalai, T., & Vinkó, J. 2013, A&A, 549, A79
Terzieva, R., & Herbst, E. 1998, ApJ, 501, 207
Todini, P., & Ferrara, A. 2001, MNRAS, 325, 726
Valiante, R., Schneider, R., Bianchi, S., & Andersen, A. C. 2009, MNRAS, 397, 1661
Valiante, R., Schneider, R., Salvadori, S., & Bianchi, S. 2011, MNRAS, 416, 1916
Verner, D. A., & Ferland, G. J. 1996, ApJS, 103, 467
Wakelam, V., Loison, J.-C., Herbst, E., et al. 2009, A&A, 495, 513
Wang, R., Carilli, C. L., Wagg, J., et al. 2008, ApJ, 687, 848
Weaver, T. A., Zimmerman, G. B., & Woosley, S. E. 1978, ApJ, 225, 1021
Wooden, D. H., Rank, D. M., Bregman, J. D., et al. 1993, ApJS, 88, 477
Woon, D. E., & Herbst, E. 1996, ApJ, 465, 795
Woosley, S. E., Hartmann, D., & Pinto, P. A. 1989, ApJ, 346, 395
Woosley, S. E., & Heger, A. 2007, Physics Reports, 442, 269
Yu, T., Meyer, B. S., & Clayton, D. D. 2013, ApJ, 769, 38